NUMERICAL MODELLING OF THE VISCO-PLASTIC BEHAVIOUR OF A WIDE AUSTENITIC STAINLESS STEEL CRACKED PLATE

C. Poussard[1], L. Le Ber[2] , C. Delaval[3] and C. Sainte Catherine[4]

[1] CEA (Commissariat à l'Energie Atomique), CEN SAC, DRN/DMT/SEMI/LEMO, F-91191 Gif-sur-Yvette, France - Email : christophe.poussard@drnsac.cea.fr
[2] CEA, CEN SAC, DRN/DMT/SEMT/LISN, F-91191 Gif-sur-Yvette, France - Email : leber@cea.fr
[3] IPSN (Institut de Protection et Sûreté Nucléaire), CEN FAR, DES/SEGREN, F-92265 Fontenay-aux-Roses, France - Email : christine.delaval@ipsn.fr
[4] CEA, CEN SAC, DRN/DMT/SEMI/LCMI, F-91191 Gif-sur-Yvette, France - Email : saintecatherine@drnsac.cea.fr

ABSTRACT

This paper presents the results of a numerical study which has been undertaken to predict the mechanical behaviour of a wide austenitic stainless steel cracked plate submitted to creep-fatigue bending load cycles at 650°C. In order to get a better understanding of the mechanical process at the crack tip and then use damage mechanics for life estimation purposes, finite element simulations of this test have been undertaken. For this, a sophisticated constitutive visco-plastic model referred to as the DID (Double Inelastic Deformation) model was used. This model, available in the finite element code CASTEM 2000 developed at CEA, is a non unified cyclic law that splits the inelastic strain into plastic and viscous strain terms. Each inelastic strain is described with a non-linear isotropic law and a non-linear kinematic hardening law. The plastic flaw rule is based on the Hill assumption and the visco-plastic behaviour is approximated with a secondary creep law. The paper addresses the multi-axial equations as well as the identification of the model parameters. The testing conditions are summarised and emphasis is given toward the results obtained with the model.

KEYWORDS

Visco-plastic Fracture Mechanics, Fatigue and Creep Damages, Constitutive Equations, Austenitic Stainless Steel, Finite Element Modelling.

INTRODUCTION

The study reported in this paper has been motivated by the fact that with the help of sophisticated multi-axial equations available in modern finite element codes, it is nowadays possible to study numerically the stresses and strains that develop in complex geometries subjected to complex loading situations. This type of analysis is particularly useful to validate our understanding of the behaviour of power plant components that may operate at high temperature and undergo cyclic loads. Furthermore, it can provide useful numerical values

that can be compared to the results of simplified analytical methods available in defect assessment procedures.

This type of approach has already been successfully used to investigate the conservatism associated with a creep-fatigue crack initiation criterion. For an austenitic stainless steel, the σ_d approach [1] postulates that the stress range $\Delta\sigma_{yy}$, calculated at a distance of 50μm from the crack tip, can be used together with visco-plastic deformation corrections to determine fatigue and creep damages to initiation. The analysis reported in [2] has shown that for a small compact tension specimen, the analytical methods proposed in available defect assessment procedures do not lead to stress and strain estimations in good agreement with precise finite element calculations. In the following, the work mentioned above is extended to the analysis of a larger component consisting of a wide austenitic stainless steel plate with a semi-elliptical crack.

DID MODEL MULTI-AXIAL EQUATIONS

The DID (Double Inelastic Deformation) model [3] available in CEA in house finite element code CASTEM 2000 [4] was used for the calculations. This model is a cyclic visco-plastic non-unified model that splits the inelastic strain into two terms :

$$\underline{\underline{\varepsilon}}_i = \underline{\underline{\varepsilon}}_p + \underline{\underline{\varepsilon}}_v$$

where $\underline{\underline{\varepsilon}}_p$ is the plastic strain and $\underline{\underline{\varepsilon}}_v$ is the viscous strain. Each inelastic strain term is described with a non-linear isotropic and a transient non-linear kinematic hardening. The plastic flow rule is based on the Hill assumption and the visco-plastic flow rule is simulated by a secondary creep law. The multi-axial equations of the model are presented in Table 1. In this form, the DID model has 17 parameters. Their significance is not discussed in this paper since it is available in [3].

IDENTIFICATION OF THE MODEL PARAMETERS

Contesti et al. [5] have identified the model parameters using an extensive database available for the 316L stainless steel at 600°C. In this study, this identification was however repeated in order to identify the parameters at 650°C, temperature corresponding to that used for the large plate specimen. This was also the opportunity to identify the model parameters for fatigue, creep and large plate specimens machined in the same batch of material.

The 17 parameters of the model are to be identified from a set of available uniaxial experiments that enable to differentiate the respective influence of each of them. It is well established that the visco-plastic strain increases when the testing strain rate decreases. Therefore, high strain rate tests are used for the identification of the plastic behaviour whilst low strain rate tensile, creep, fatigue and fatigue relaxation tests are used for the identification of the visco-plastic behaviour. The identification of the parameters was achieved with IDENT 1D, software developed at CEA to perform reliable and automatic identification of sophisticated constitutive equations such as the DID model. References [6] and [7] give a full description of the strategies used in IDENT 1D to identify the DID model parameters.

In IDENT 1D, the isotropic plastic parameters are first identified from high strain rate tests using an automatic linear regression to determine the first cycle yield stress, the stabilised yield stress and the cyclic hardening. The kinematic parameters are then pre-identified using a basic analytical procedure. A numerical scheme is then used to optimise the plastic parameters. First, the isotropic parameters are fixed and a cost function is minimised to optimise the kinematic parameters. This scheme is then used to optimise the isotropic parameters with fixed kinematic parameters until convergence is obtained. A similar procedure is then used to identify the visco-plastic parameters for low strain rate tests. The coefficients of a Norton type creep law are first approximated using a linear regression to the secondary creep stage test results. Similarly to the plastic parameters, these coefficients are then used to pre-identify the visco-plastic isotropic and

kinematic parameters. The creep law is then integrated in order to optimise the coefficients of the Norton creep law. A full optimisation of the whole visco-plastic parameters is finally performed.

For the 316L(N) steel at 650°C investigated in this study, 3 fatigue tests performed at strain rates ranging between 0.1 and 0.001%.s^{-1} and 3 creep tests performed with a nominal applied stress ranging between 170 and 210 MPa were selected for the identification. Figure 1 (fatigue test at $\dot{\varepsilon}$=0.01%.s^{-1}) shows that a very good correlation between the fatigue test results and the DID constitutive equation can be obtained for the material. Figure 2 gives a comparison between the identified model and the creep test data. The model is found to underestimate the creep strain for low applied loads whilst it is overestimated for high applied loads. Table 2 gives the set of optimised parameters identified for the material at 650°C.

SPECIMEN, TESTING PROCEDURE AND FINITE ELEMENT MODELLING

The model previously outlined was used to study the visco-plastic behaviour of a large scale experiment which consists of a wide cracked plate machined in the batch of material for which the parameters have been identified. The plate with the semi-elliptical surface notch is subjected to over 3000 creep-fatigue bending cycles at 650°C with a one hour dwell. The geometry and the loading conditions are shown in Figure 3 and detailed in [8]. The test is carried out under imposed load conditions with ΔF=17kN, R=-0.26 during the fatigue pre-cracking loading sequence and with ΔF=28kN, R=-1 and a dwell period of 1 hour during the creep-fatigue loading sequence. A first interpretation of the test results has shown that the global parameters measured during the test are significantly time dependent [8].

At this preliminary stage of the investigation, costs computations have been reduced : only a 2D finite element analysis of one half of the longitudinal plate section has been achieved. Figure 4 shows the mesh together with the boundary conditions assumed in the calculations. The mesh is constituted with 610 isoparametric quadratic elements and plane strain is assumed. The mesh in the vicinity of the crack tip is refined in such a way that a good description of the local stress and strain fields can be obtained at a distance of 50μm from the tip, characteristic distance used in the σ_d approach [1] to predict creep-fatigue crack initiation. The crack depth corresponds to the dimension of the crack obtained at the end of the fatigue pre-cracking loading sequence (a_{cf}=7.9mm) in the thickness direction. The bending moment is simulated with 2 vertical nodal loads of opposite signs together with underformable elements at the upper end of the plate to simulate the stiff rigid grips used in the experiment. The height of the mesh corresponds the length of the plate submitted to an homogeneous temperature of 650°C. Finally, contact elements are used along the crack mouth in order to account for crack closure effects produced by the negative load ratio applied in the test.

RESULTS

The first result that may be reported from this simulation concerns the crack closure effect which is not well understood in this type of experiment. Figure 5 presents the evolution of the CMOD (crack mouth opening displacement) versus applied load calculated for 10 fatigue cycles at R=-2. The hysteresis loops are found to be significantly affected by crack closure effects. According to Elber [9], these loops can be used to derive (Figure 6) a crack closure factor U ($U=\Delta K_{eff}/\Delta K$) which expresses the ratio between the effective SIF (Stress Intensity Factor) range over the total SIF range. Elber has demonstrated that this factor is also directly proportional to the effective load range over the total load range ($U=\Delta L_{eff}/\Delta L$), the effective load range being defined by the range of load corresponding to the maximum load and the load producing a full opening of the crack. The computed results are found to be less pessimistic than proposed in the A16 document [1]. For low R ratios, the results compare favourably well with the model determined by Polvora for 316L(N) at high temperatures [10].

Figure 7 gives the evolution of the crack tip opening stress σ_{yy} at a distance of 50μm as a function of the total opening strain ε_{yy}. The doted line corresponds to the fatigue cycles (10 computed cycles at R=-0.26) whilst the plain line corresponds to the creep fatigue cycles with 1 hour dwell (30 cycles at R=-1). The material is

found to harden during the fatigue cycles whilst the cumulated total strain becomes significant. As for the creep-fatigue loading regime, it is found that the stress relaxation during the dwell is significant. Each dwell period produces a stress relaxation of about –150MPa. The maximum stress at the beginning of each dwell period is also found to decrease smoothly during the test. The hysterisis loops shift progressively close to an average stress value of –200 MPa. This is explained by the stress relaxation that occurs during the dwell which is not fully restored by the load reversal at the beginning of each dwell period. Although not shown in the paper, a similar behaviour is obtained on the back surface of the plate (figure 4) : the hysterisis loops shift progressively towards an average stress of –25MPa. Due to the presence of the singularity, the shift is more important at 50μm than on the back surface.

Figure 8 compares the amount of relaxed opening stress ($\Delta\sigma_{yy}$) over the creep-fatigue cycles. Computation are reported for dwell periods of 1 and 3 hours. Also shown on this figure are the results obtained for simulations including or not the influence of fatigue pre-cracking (10 fatigue cycles at R=-0.26) calculated prior to the creep fatigue cycles). As expected, the amount of relaxed stress is more pronounced for the 3 hour dwell calculations than for the 1 hour dwell calculations. The influence of the fatigue cycles prior to the creep-fatigue loading sequence is important for the first 5 cycles. This also corresponds to the maximum value of $\Delta\sigma_{yy}$. These observations are related to the cyclic hardening of the material which is readily saturated at a distance of 50μm from the crack tip. A similar analysis has been performed on the back surface of the plate : it does not exhibit the same behaviour since the material continues to cyclically harden over the number of calculated cycles.

Finally, Figures 9 and 10 show the evolution of the total strain as a function of time for the loading conditions mentioned above at a distance of 50μm from the crack tip and at the back surface of the plate. A positive strain accumulation and a negative one are observed at the crack tip and at the back surface of the plate, respectively. An analysis of each strain terms individually (elastic, plastic and visco-plastic) reveals that the plastic strain range readily stabilises and then decreases whilst the visco-plastic strain smoothly increases with the number of cycles. Also, the shorter the dwell period, the greatest the accumulated strain becomes. This means that it is mainly due to the strain developed at crack tip during the relaxation phase and is probably very dependant upon the structure.

CONCLUSIONS

2D finite element simulations of a large austenitic stainless steel centre cracked plate subjected to creep-fatigue bending cycles at 650°C have been undertaken using a sophisticated constitutive model that allows to account for both the plastic behaviour of the material and the creep deformations that arise at such temperatures. As a prerequisite, the model parameters, 17 parameters, have been identified from a set of uniaxial fatigue and creep test results obtained from the same batch of material.

The constitutive equations of the model are found to well reproduce the plastic behaviour of the material whilst they underestimate the creep deformation for low applied loads and overestimate the creep strain for high applied loads. The results of the simulations show that the crack closure factor may not be as conservative as proposed in the A16 document. An analysis of the crack tip opening strain and stress shows that the fatigue cycles applied to the specimen in order to fatigue pre-crack the plate affect substantially the behaviour of the plate. The material is found to cyclically harden readily at the crack tip. The stress at the beginning of each dwell period is found to decrease smoothly with the applied cycles. This is explained by the fact that the stress reversal does not restore completely the stresses relaxed during the dwells. It is concluded that this type of approach can now be used to improve and reduce the conservatism associated with defect assessment procedures.

REFERENCES

[1] Drubay, B. et al., 1997, *A16 : A French Guideline for Defect Assessment and Leak Before Break Analysis*, ASME, Proc. of ICONE 5, 26-30/05, Nice, FRANCE.

[2] Laiarinandrasana, L. and Piques, R., 1998, *Creep-fatigue crack initiation in 316L stainless steel : comparison between stress and strain calculation methods*, Proc. of SISSI 3, pp. 201-208, Saclay, FRANCE.

[3] Cailletaud, G. and Sai, K., 1995, *Study of plastic/viscoplastic models with various inelastic mechanisms*, Int. Journal of Plasticity, Vol. 11, pp. 991-1005.

[4] CASTEM 2000, 1998, Commissariat à l'Energie Atomique, DRN/DMT/SEMT/LM2S, 91191, Gif sur Yvette, FRANCE

[5] Contesti, E. and Cailletaud, G., 1989, *Description of creep-plasticity interaction with non-unified constitutive equations*, Nuclear Engineering and Design, Vol. 116, pp. 265-280.

[6] Le Ber, L., Champain, E., Nicolas, L. and Sainte Catherine, C., 1997, *Ident 1D : Identification of material constitutive parameters*, Proc. of ECF 12, Sheffield, UK, 14-18 Sept. 1998, pp. 423-428.

[7] Le Ber, L., Cotoni, V., Nicolas, L. and Sainte Catherine, C., 1998, *Ident 1D : A novel software tool for an easy identification of material constitutive parameters*, Nuclear Engineering and Design, 186, pp. 343-352.

[8] Poussard, C. et al., 1998, *Creep-fatigue crack growth in austenitic stainless steel centre cracked plates at 650°c - Part I and II*, Proc. of SISSI 3, pp. 131-138 and pp. 271-279, Saclay, FRANCE.

[9] Elber, W., 1971, *The significance of fatigue crack closure, damage tolerance in aircraft structures*, ASTM STP 486, pp 230-242.

[10] Polvora, J.P., 1998, *Propagation de fissure à haute température dans un acier inoxydable austénitique*, Ph. D thesis, Ecole des Mines de Paris, Rapport CEA R 5802.

TABLES

Table 1 : Multi-axial equations of the DID model

PLASTIC STRAIN MECHANISM	VISCO-PLASTIC STRAIN MECHANISM
Scale yielding equations	
$f_p = J_2(\underline{\underline{\sigma}} - \underline{\underline{X}}_p) - R_p$	$f_v = J_2(\underline{\underline{\sigma}} - \underline{\underline{X}}_v) - R_v$
Flow rules	
$\underline{\underline{\dot{\varepsilon}}}_p = \frac{3}{2}\dot{p}\frac{\underline{\underline{\sigma}}' - \underline{\underline{X}}_p'}{J_2(\underline{\underline{\sigma}} - \underline{\underline{X}}_p)}$ $\dot{p} = \dot{\varepsilon}_{eq} = \sqrt{\frac{2}{3}\underline{\underline{\dot{\varepsilon}}}_p : \underline{\underline{\dot{\varepsilon}}}_p}$ p is the cumulated plastic strain	$\underline{\underline{\dot{\varepsilon}}}_v = \frac{3}{2}\dot{v}\frac{\underline{\underline{\sigma}}' - \underline{\underline{X}}_v'}{J_2(\underline{\underline{\sigma}} - \underline{\underline{X}}_v)}$ $\dot{v} = \dot{\varepsilon}_{eq} = \left\langle \frac{f_v}{K} \right\rangle^n$ v is the cumulated viscoplastic strain
Isotropic strain hardening functions	
$R_p = R_{p0} + Q_p\left(1 - \exp(-b_p p)\right)$	$R_v = R_{v0} + Q_v\left(1 - \exp(-b_v v)\right)$
Kinematic strain hardening functions	
$\underline{\underline{X}}_p = \frac{2}{3}C_{pi}\underline{\underline{\alpha}}_{pi} + \frac{2}{3}C_{vpi}\underline{\underline{\alpha}}_{vi}$ $\underline{\underline{\dot{\alpha}}}_{pi} = \underline{\underline{\dot{\varepsilon}}}_p - d_{pi}\underline{\underline{\alpha}}_{pi}\dot{p}$	$\underline{\underline{X}}_v = \frac{2}{3}C_{vi}\underline{\underline{\alpha}}_{vi} + \frac{2}{3}C_{vpi}\underline{\underline{\alpha}}_{pi}$ $\underline{\underline{\dot{\alpha}}}_{vi} = \underline{\underline{\dot{\varepsilon}}}_v - d_{vi}\underline{\underline{\alpha}}_{vi}\dot{v}$

' is the deviatoric part of the tensors, $\langle\ \rangle$ is the positive part and $\underline{\underline{\ }}$ the second order tensors

Table 2 : Optimised parameters identified for the 316L(N) austenitic stainless steel at 650°C

		PLASTIC STRAIN MECHANISM			VISCO-PLASTIC STRAIN MECHANISM		
Flow rules parameters		1	Young's modulus E (MPa) Poisson's ratio ν	170 000 0.3	2	Norton creep stress K	878.319
		-	Hill assumption, no parameter	-	3	Norton creep exponent n	6.63
Isotropic strain hardening parameters	Initial plastic flow stress	4	$R_{p0.2}$ (MPa)	29.2	5	R_{v0} (MPa)	0.001
	Plastic flow stress variation	6	Q_p (MPa)	106.232	7	Q_v (MPa)	21.815
	Cyclic hardening rate	8	B_p	20.882	9	B_v	10.161
Kinematic strain hardening parameters	Strain hardening parameters	10 11	C_{p1} C_{p2}	45664.6 547370.7	12 13	C_{v1} C_{v2}	43499.3 533751.8
	Dynamic recovery parameters	14 15	D_{p1} D_{p2}	622.0 11784.4	16 17	D_{v1} D_{v2}	759.6 12945.5
Plastic and visco-plastic kinematic hardening coupling parameters *		18	C_{vp1}	0	19	C_{vp2}	0

* C_{vp1} and C_{vp2} are not considered in this version of the model

FIGURES

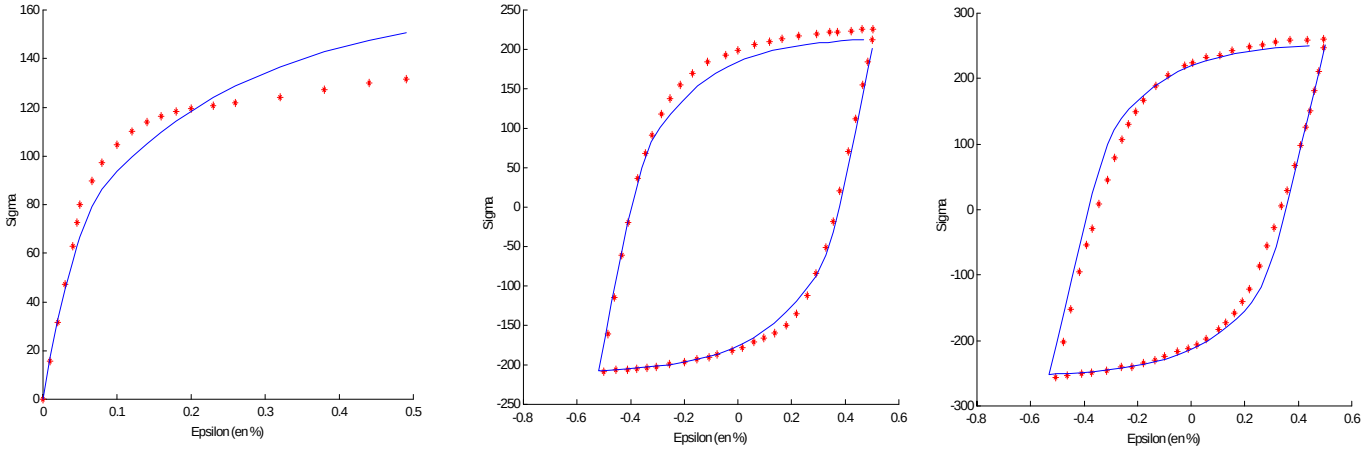

(a) first loading (b) 4th cycle (c) Stabilised cycle

(∗ = experimental data — = numerical prediction)

Figure 1 : Comparison between experimental fatigue test results at $\dot{\varepsilon}$=0.01%.s^{-1} and predicted behaviour

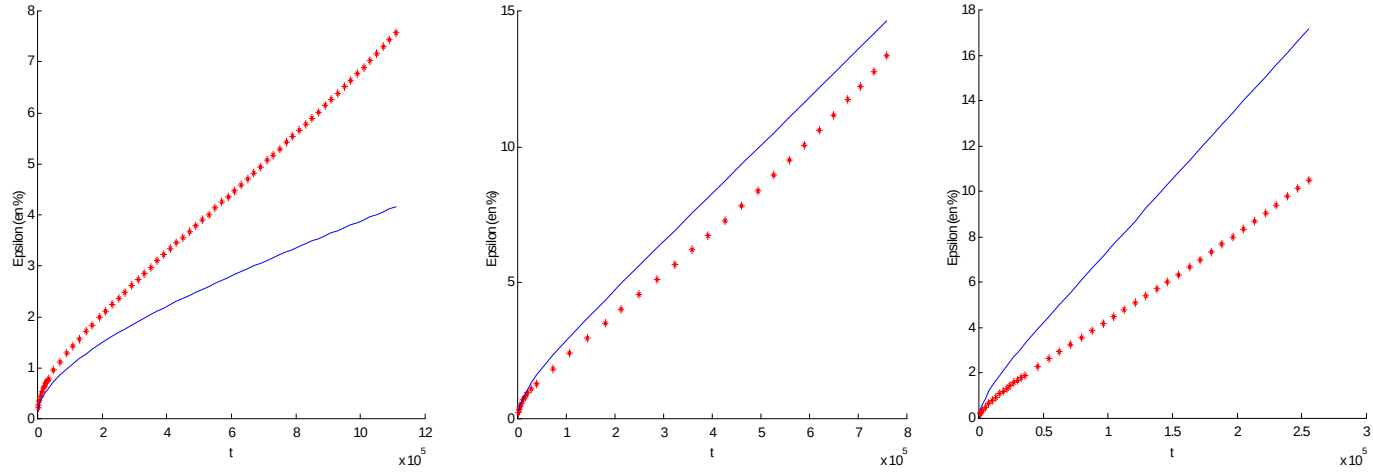

(a) creep test at σ=170 MPa (b) creep test at σ=190 MPa (c) creep test at σ=210 MPa

(∗ = experimental data — = numerical prediction)

Figure 2 : Comparison between experimental creep test results and predicted behaviour

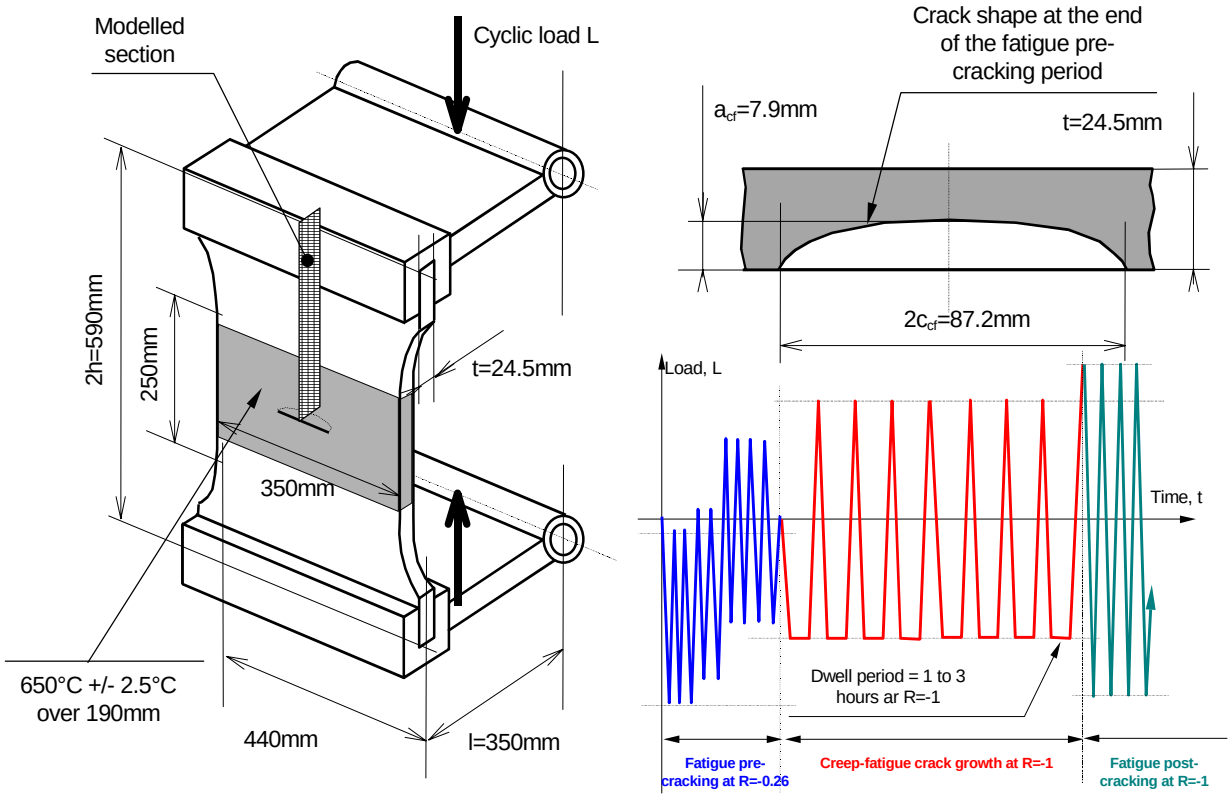

Figure 3 : Plate specimen, experimental arrangement and loading conditions

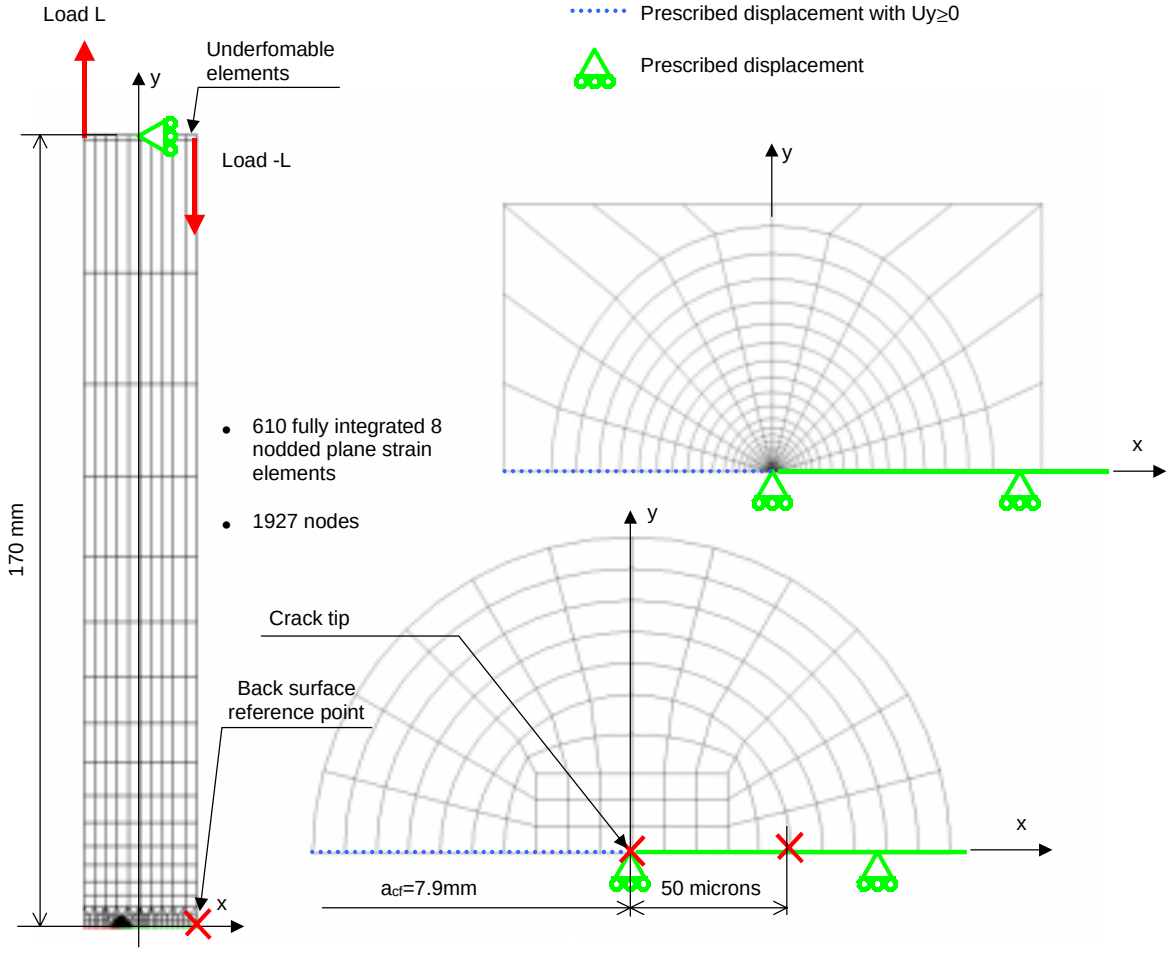

Figure 4 : 2D finite element mesh of the plate and boundary conditions

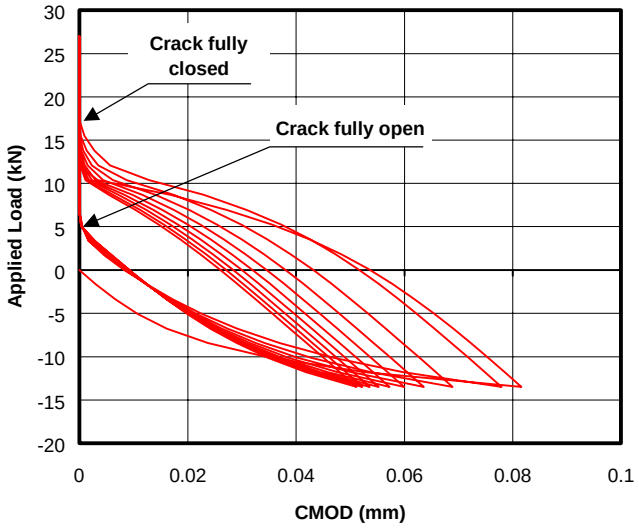

Figure 5 : Applied load versus CMOD at R=-2

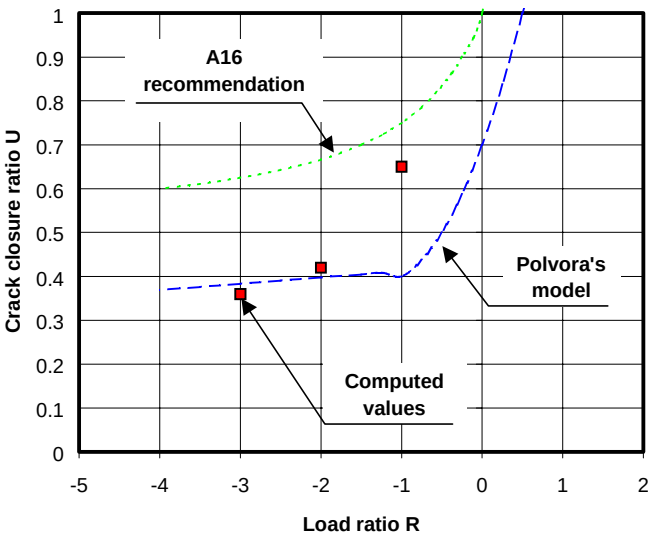

Figure 6 : Crack closure predictions

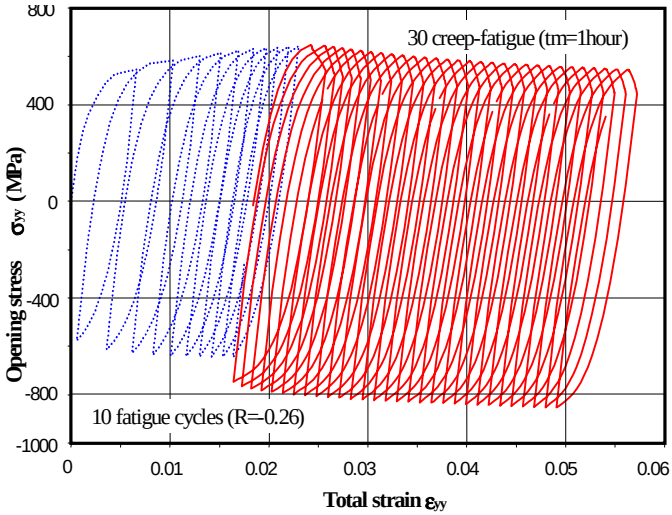

Figure 7 : Opening stress versus total opening strain at 50µm

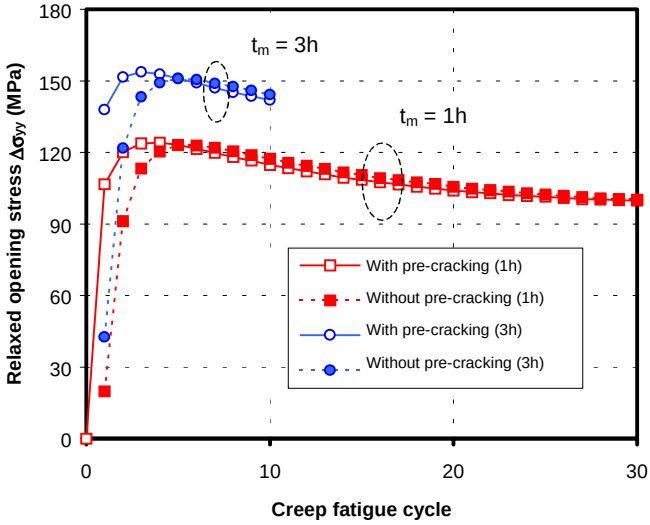

Figure 8 : Opening stress relaxation at 50µm

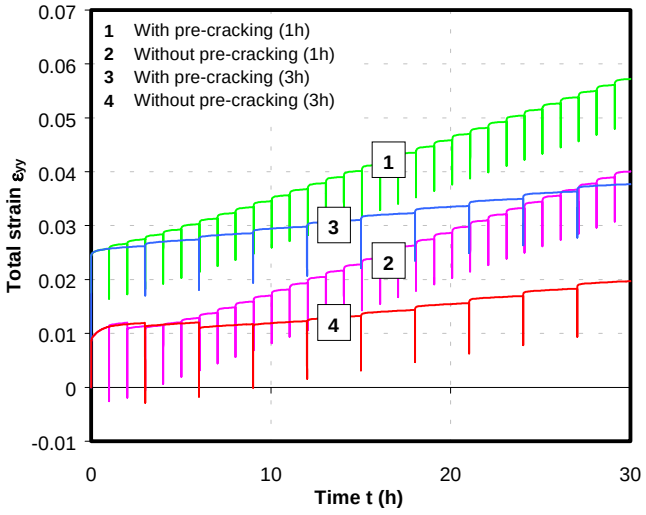

Figure 9 : Total opening strain at 50µm

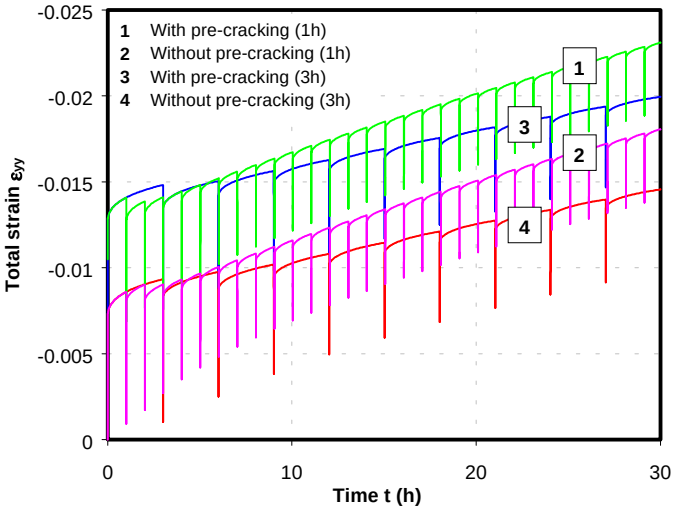

Figure 10 : Total opening strain on the back surface